Point defects: Their influence on electron trapping, resistivity, and electron mobility-lifetime product in $CdTe_xSe_{1-x}$ detectors

R. Gul,[1,2] U. N. Roy,[1] S. U. Egarievwe,[2] A. E. Bolotnikov,[1] G. S. Camarda,[1] Y. Cui,[1] A. Hossain,[1] G. Yang,[1] and R. B. James[1]
[1]*Brookhaven National Laboratory, Upton, New York 11973, USA*
[2]*Alabama A&M University (ECMIT), Normal, Alabama 35762, USA*

(Received 23 October 2015; accepted 24 December 2015; published online 8 January 2016)

In this research, we assessed the abundance of point defects and their influence on the resistivity, the electron mobility-lifetime ($\mu\tau_e$) product, and the electron trapping time in CdTeSe crystals grown under different conditions using the traveling heater method. We used current-deep level transient spectroscopy to determine the traps' energy, their capture cross-section, and their concentration. Further, we used these data to determine the trapping and de-trapping times for the charge carriers. The data show that detectors with a lower concentration of In-dopant have a higher density of A-centers and Cd double vacancies (V_{Cd}^{--}). The high concentrations of V_{Cd}^{--} and A-centers, along with the deep trap at 0.86 eV and low density of 1.1 eV energy traps, are the major cause of the detectors' low resistivity, and most probably, a major contributor to the low $\mu\tau_e$ product. Our results indicate that the energy levels of point defects in the bandgap, their concentrations, capture cross-sections, and their trapping and de-trapping times play an important role in the detector's performance, especially for devices that rely solely on electron transport.
 [http://dx.doi.org/10.1063/1.4939647]

I. INTRODUCTION

The promising optoelectronic properties of II-VI semiconductor materials make them attractive for research and for the development of commercial technologies. CdTe, CdZnTe, CdMnTe, CdSe, CdS, and CdTeSe presently are considered as the best candidates as room-temperature radiation detectors for usages in national security, monitoring, and assuring the non-proliferation of nuclear materials. They also are invaluable as imaging devices for nuclear medicine and research in space, for light-emitting diodes, and as multi-layers and hetero-structures for optoelectronic devices.[1] So far, most research and development has focused on CdZnTe,[2,3] and its related II-VI materials. Presently, CdTeSe is becoming an increasingly attractive alternative to CdZnTe. The successful achievement of a controllable band-gap, the 1.3 times higher binding energy of the CdSe crystals' structure than that of CdTe, along with the 0.9 times shorter lattice-constant of CdTe, makes CdSe crystals an excellent alternative to using CdTe and its alloys. Furthermore, their closely packed system results in fewer Cd vacancies (V_{Cd}^{--}). In addition, the tight bonding of CdSe-based materials makes them very suitable for use as radiation detectors, because they are less susceptible to damage from handling. During the growth of these crystals especially from the melt, the segregation coefficient makes a major contribution to assuring a high degree of uniformity in the crystals. Comparing the segregation coefficients of both systems, the Zn in CdTe system has a value ≥ 1, while that of Se in CdTe is ~ 1; hence the alloy composition of CdTeSe crystals is more uniform than those of CZT. This high elemental homogeneity in the ingot has the potential to greatly enhance the yield of detector material. Notably, the high uniformity of the CdTeSe (CTS) ingots is expected to entail at least a two-fold reduction in production costs compared to CZT for applications such as large-area substrates and large-volume detector material.[4]

The nature of imperfections in such crystals, and the content and types of extended- and point-defects have been extensively studied, as has their effects on the electrical transport properties and the material's performance as a radiation detector.[5,6] In our research, we grew ingots of cadmium telluride selenide via the Traveling Heater Method (THM) at Brookhaven National Laboratory's crystal growth facility. CTS crystals with different compositions of raw material, $CdTe_xSe_{1-x}$ with $x = 0.90$ with a high concentration of In-dopant, and $x = 0.95\%$ with a low concentration of In-dopant were characterized for point defects, using the current-deep level transient spectroscopy (i-DLTS) technique. Further details about the crystals' growth parameters and conditions were reported by Roy *et al.*[7] The i-DLTS experimental setup is described by Gul *et al.*[5] In our previous research,[8] we identified different types of point defects in these crystals. In this research, we identified the point defects within the crystal's band-gap in two types of CTS detectors grown under different conditions. In the next step, we used the data on the parameters of the point defects to determine the times taken by the defects to trap and then de-trap the charge carriers. Finally, we related i-DLTS data and the detector's performance with the electrical resistivity of the CTS material and the values of the material's $\mu\tau_e$-product.

II. EXPERIMENTAL DETAILS

We used two sets of planar detectors, CTS-2B ($CdTe_xSe_{1-x}$ with $x = 0.90$ with high concentration of In

dopant), and CTS-4G ($CdTe_xSe_{1-x}$ with $x = 0.95\%$ with a low concentration of In dopant). Table I lists the specifications, the resistivity, and the values for the $\mu\tau_e$-product. After measuring the resistivity and obtaining the $\mu\tau_e$ product using Hecht equation-fitting, the i-DLTS experiments were run to characterize the point defects within the band-gap of the two types of CTS detectors.

For collecting the i-DLTS experimental data, the CTS detector was mounted on the cold finger in a He-closed cryogenic system, and the base-line correction was taken at room temperature. The samples were cooled to 13 K, and then heated to 400 K, in average steps of 1 ± 0.1 K. In a complete run, we acquired about 30 data points, each of which was collected at a fixed stable temperature, and the transients were collected at every individual step. At a stable temperature, the traps were filled using an 822 nm laser. With a pulse generator, we obtained a square pulse-shaped signal, 2 ms-wide, and a period of 1 s. To identify and distinguish the traps, we applied biases of 1 and 10 V across the detector. We calculated these i-DLTS parameters, i.e., the activation energies, densities, and capture cross-sections; the point defects were calculated using the model by Li.[8] The data also were analyzed to determine the trapping and de-trapping times for the charge carriers.

III. RESULTS AND DISCUSSION

We analyzed the transient current obtained from the i-DLTS measurements to determine the energy level/trap (E_t), trap density (N_t), and the capture cross-section (σ), as shown in Figs. 1–4. To clarify the effects of the point defects on the detector's performance, we used their parameters to calculate the trapping- and de-trapping times (t_t and t_{dt}) as shown in Fig. 5, respectively, for the charge carriers by each trap; the results also are compiled in Tables I and II. To better explain the information obtained from the i-DLTS experiments for the point defects, we separately discuss these defects' parameters (E_t, N_t, and σ), and the indirect influence of these parameters on the material's electrical properties and the detectors' performance by focusing on the times for trapping and de-trapping of the charge carriers.

A. i-DLTS parameters (energy, capture cross-section, and density of traps)

Fig. 1 shows the i-DLTS plots denoting the point defects present in CTS-2B (Fig. 1(a)), and CTS-4G (Fig. 1(b)); in addition, Fig. 2 shows the Arrhenius plots. We used the slope and intercept for each trap to calculate the trap's E_t and σ, respectively. The concentration of the trap is calculated from

TABLE I. Physical- and electrical-transport parameters for two groups of detectors: CTS-2B and CTS-4G.

	CTS-2B	CTS-4G
Area (mm^2)	18.3	39.0
Thickness (mm)	1.8	1.8
Resistivity (Ω cm)	$4–5 \times 10^8$	$4–5 \times 10^9$
$\mu\tau_e$ product (cm^2/V)	4.0×10^{-3}	2.6×10^{-2}

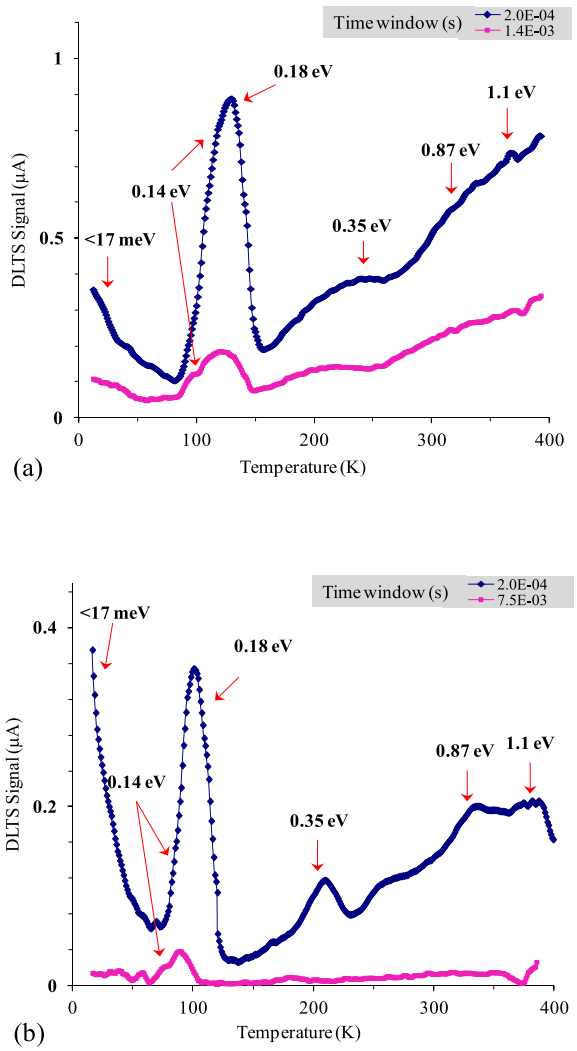

FIG. 1. I-DLTS plots showing point defects for two different time windows with a 2 ms pulse width at 1 V applied bias for (a) CTS-2B and (b) CTS-4G.

the i-DLTS plot's current-peak value and the time window for the transient current.

There are six different types of measurable energy-traps from a few meV to the deepest trap near the conduction band; the calculated activation energies for the traps are (13–17) meV, 0.14 eV, 0.18 eV, 0.35 eV, 0.87 eV, and 1.1 eV. In Fig. 3, we plotted the σ values for each level, showing that the values vary exponentially with an increase in energy, with the lowest value of $\sim 10^{-19}$ cm^2 for the 17 meV shallow trap, and 10^{-11} cm^2 for the deepest energy level of 1.1 eV.

Deep traps are the focus of our research, so we divided them into two groups: shallow, medium, and deep traps.

1. Shallow- and medium-energy traps

As observed in Figs. 1(a) and 1(b), a shallow trap at around 17 meV with σ of 10^{-19} cm^2 is located in the low-temperature region below 50 K. The trap is probably related to the interstitial point defects induced by Cl, Al, or Ni as donor impurities that are present, respectively, in concentrations of <30 ppb, 39 ppb, and 100 ppb in the raw material.

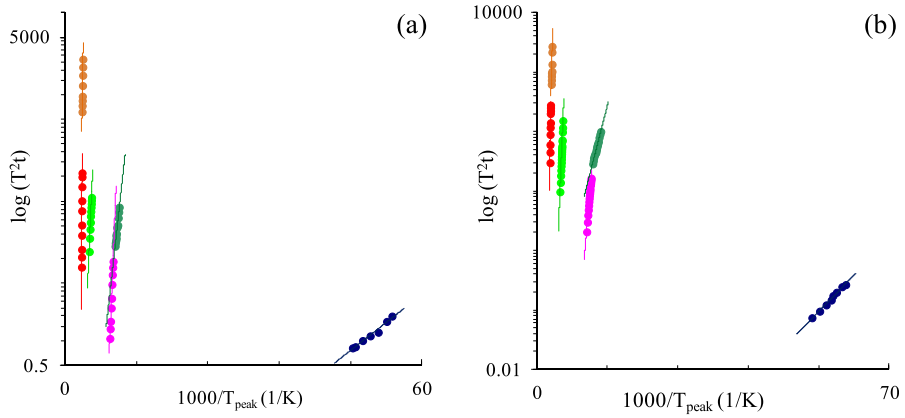

FIG. 2. Arrhenius plots for different point defects in two detectors: (a) CTS-2B and (b) CTS-4G.

The respective densities of these shallow donors are $\sim 2 \times 10^{13}$ cm^{-3} and 1×10^{13} cm^{-3} in the CTS-2B and CTS-4G detectors.

We identified two different complex defects $(In^{+}—V_{Cd}^{--})^{-}$, called A-centers, located around 100 K, with activation energies of 0.14 eV and 0.18 eV. Table II gives the values of σ, shown in Fig. 3. They differ by almost one order-of-magnitude, being, respectively, 5×10^{-17} cm^2 and 1×10^{-16} cm^2. The trap around 0.18 eV is a well-known A center; it is a hole trap, a complex of the V_{Cd}^{--} with the In dopant, while the 0.14 eV trap is a different complex of V_{Cd}^{--} with group-III elemental impurities. The GDMS data (not included here) on these THM-grown CTS crystals indicated relatively high concentrations of Al, Ge, and Si; hence, there is a high probability of the formation of a 0.14 eV complex between V_{Cd}^{--} and the Al interstitials. The closeness of the values of the concentrations and of the activation energies makes it difficult to distinguish between the two neighboring traps. Two A-centers with different origins can easily be distinguished for the high time-window shown in Fig. 1. The densities of both A-centers are almost the same ($\sim 3 \times 10^{13}$ cm^{-3}) in detector CTS-2B. On the other hand, this is not the case in CTS-4G; the concentration of the In-related A-center is a little lower than the Al-related A-center. The high concentration of the 0.18 eV traps in CTS-2B is probably due to the high concentration of In dopant.

The next trap, a medium-energy hole trap around 200 K, is shown in Fig. 2; it is related to Cd- vacancies[9] (V_{Cd}^{--}) with

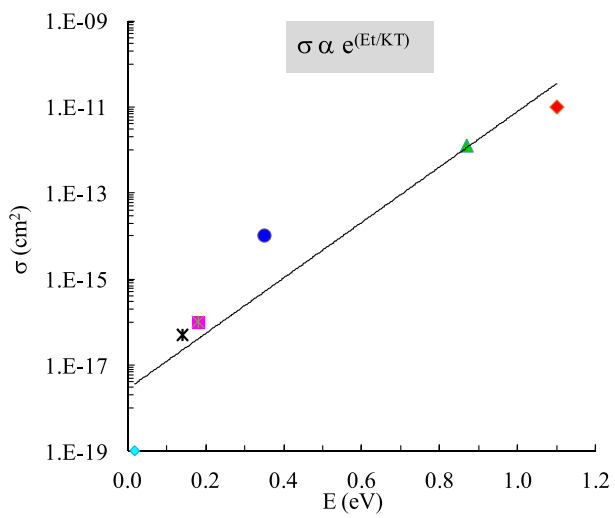

FIG. 3. The activation energies and the corresponding capture cross-sections of charge carriers for each trap.

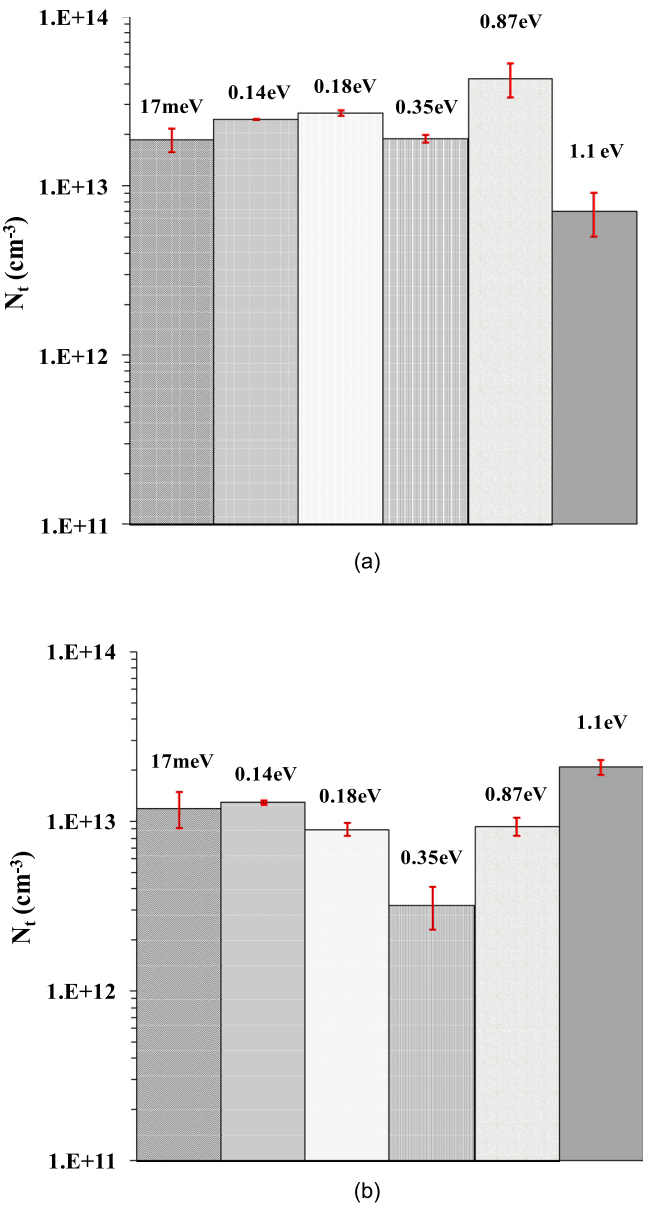

FIG. 4. Comparison of the densities of point defects in (a) CTS-2B and (b) CTS-4G.

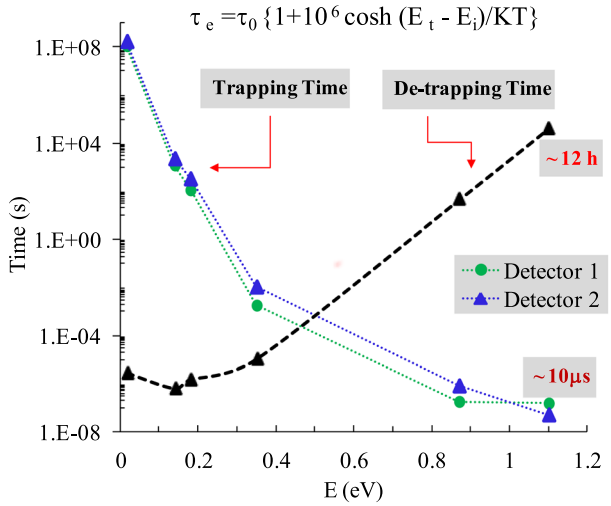

FIG. 5. Trapping and de-trapping times of point defects for the charge carriers in two types of CTS detectors.

activation energy of 0.35 eV and a σ of 1×10^{-14} cm^2. This trap was identified by others[10–12] at $E_v + 0.4$ eV, as majority carrier trap in SCLS analyses, in p-type Ge- and Sn-doped CdTe detectors. The concentration of V_{Cd}^{--} in CTS-2B is $\sim 2 \times 10^{13}$ cm^{-3}, while the value is lower, at 3×10^{12} cm^{-3} for detector CTS-4G. The variation in concentrations of the A-centers and V_{Cd}^{--} in the two detectors indicates that dopant level is not enough to compensate the V_{Cd}^{--} and hence may be one of the reasons that the 10^{10} Ω cm resistivity that is preferred for room-temperature radiation detectors is not attained.

2. Deep-energy traps

At temperatures above room-temperature, i-DLTS measurements show two deep traps, 0.87 and 1.1 eV with σ values of $\sim 10^{-12}$ cm^2 and 10^{-11} cm^2, respectively; they are identified in both CTS detectors as Fig. 1 shows. The density of the 0.87 eV trap in CTS-2B and CTS-4G is 4×10^{13} and 9×10^{12} cm^{-3}, respectively, which is a difference of less than an order-of-magnitude. Comparing the concentration of all identified traps in CTS-2B, the 0.87 eV trap has the highest concentration. Z′azvorka *et al.* (2013) in their study of the electrical response to infrared illumination of CdTe/CdZnTe detectors reported a 0.85 eV as an electron trap, below the conduction band.[13]

TABLE II. Trapping and de-trapping times of charge carriers from the traps for two groups of detectors: CTS-2B and CTS-4G.

		Trapping time (s)		
E_t	σ (cm^2)	CTS-2B	CTS-4G	De-trapping time (s)
17 meV	$\sim 10^{-19}$	1.1×10^{8}	1.7×10^{8}	2.9×10^{-6}
0.14 eV	5×10^{-17}	1.2×10^{3}	2.3×10^{3}	6.7×10^{-7}
0.18 eV	1×10^{-16}	1.1×10^{2}	3.3×10^{2}	1.6×10^{-6}
0.35 eV	1×10^{-14}	1.8×10^{-3}	1.1×10^{-2}	1.1×10^{-5}
0.87 eV	1×10^{-12}	1.8×10^{-7}	8.3×10^{-7}	4.7×10^{1}
1.1 eV	1×10^{-11}	1.5×10^{-7}	5.2×10^{-8}	4.5×10^{4}

The second deep trap in the 350–400 K range is the deepest energy trap determined from the i-DLTS data; it has energy of 1.1 eV with σ value of $\sim 10^{-11}$ cm^2. The value of the capture cross-section, as mentioned above, is very high compared to that of all other traps, indicating that 1.1 eV trap principally is responsible for trapping the charge carriers in these detectors. The density of the traps calculated from the i-DLTS data is around 7×10^{12} and 2×10^{13} cm^{-3}, respectively, in CTS-2B and CTS-4G. As the bar-plots in Fig. 4 show, compared to other traps present in CTS-4G, the 1.1 eV trap is a hole trap and has a relatively high concentration. We identified and reported a 1.1 eV trap in CZT, CdMnTe-, and CdMgTe- detectors which originated from a high concentration of small Te-rich secondary phases.[9] In our previous published work,[14] we reported polarization in the regions with high position space charge, and also found some hole-related polarization behavior in CZT detectors. Polarization in volumes with a high concentration of defects at 1.1 eV provides further evidence that this defect is a hole trap.[15] Castaldini[16] reported that the 1.1 eV trap below the conduction band originated by Te vacancies, rather than associated with Te-rich secondary phases.

B. Point defects and the resistivity of the detectors

After detailing the concentration of traps in two types of detectors, and comparing the resistivities of CTS-2B (4–5 × 10^8 Ω cm) and CTS-4G (4–5 × 10^9 Ω cm), we can relate the traps, their densities, and the resistivity of the two detectors. The results of the data on density and the resistivity of the two types of detectors, indicate that the high concentration of 1.1 eV traps (CTS-4G) is one of the major causes for the detectors' high resistivity. On the other hand, the data analysis indicates that the low concentration of A-centers, V_{Cd}^{--}, and the 0.87 eV deep trap in CTS-4G makes its resistivity about one order-of-magnitude higher than that of CTS-2B.

C. The effects of point defects on trapping and de-trapping times

Point defects, their concentrations, and the capture cross-sections for the charge carriers influence the trapping of charge carriers by the traps, and hence, the charge carriers' lifetime. Shallow electron traps and medium-energy hole traps (A-centers and V_{Cd}^{--}), which have σ values less than 10^{-14} cm^2, have minimal effects on $\mu\tau$, suggesting that they contribute negligibly towards the performance of detectors operating at room temperature, other than their role on the electrical resistivity. As discussed in Sec. III B, the 0.87 and 1.1 eV traps, respectively, have σ values of $\sim 10^{-12}$ and 10^{-11} cm^2, and hence they probably are major contributors in the trapping of charge carriers.

There still is a need for some quantitative results to relate the effects of the traps on the lifetime of charge carriers, which directly affects the $\mu\tau$-product, and hence the detectors' performances. For this reason, we calculated the times for the trapping and de-trapping of charge carriers for each trap from the i-DLTS data.

The trapping time, t_t, is calculated by using the following equation:[17]

$$t_t \sim t_o[1 + 10^6 \cosh\{(E_t - E_i)/KT\}], \quad (1)$$

where $t_o = \{N_t V_{th} \sigma\}^{-1}$.

E_t is the energy of the point defect/ level of the trap, E_i is the intrinsic Fermi level, K is the Boltzmann constant, T is the temperature, and V_{th} is the thermal velocity of the carriers.

The trapping time is determined from the emission rate (e_n) of the charge carriers from the laser- filled traps by using

$$e_n \sim T^2 \sigma \, Exp\,(-E_t/KT), \quad (2)$$

where $t_{dt} \sim \{e_n\}^{-1}$.

To illustrate the variation in trapping and de-trapping times with the corresponding energies, we compiled the data in Table II and plotted them in Fig. 5. The trapping time decreases hyperbolically with increasing activation energies of the traps, as illustrated by the plots, and indicates that the deep traps are faster in trapping the charge carriers than are the shallow traps. The highest value of the charge trapping time (~hours) is calculated for the 17 meV donor trap, while the lowest value of about 10 μs is calculated for the 1.1 eV trap. The trapping time analysis of the point defects indicates that V_{Cd}^{--} captures the charge carriers in a few milliseconds, while 1.1 eV and 0.87 eV trap carriers within micro seconds, and so these deep-level defects can significantly affect the output signal.

It is evident that the trapping times for most of traps, except 1.1 eV, are larger for CTS-4 G than for CTS-2B; this means that due to the higher concentrations of energy traps in CTS-2B, they are responsible for the relatively shorter times for trapping of charge-carriers. The trapping times in CTS-4 G for 17 meV, 0.14 eV, 0.18 eV, 0.35 eV, and 0.87 eV are almost 1.5×, 2×, 3×, 6×, and 4.6× times larger, on the other hand for 1.1 eV trap, it is 3 times smaller than that for CTS-2B. The higher $\mu\tau_e$ product for CTS-4G (2.6×10^{-2} cm^2/V) is related to the higher values of trapping times in detector CTS-4G. Comparing the $\mu\tau_e$ and the trapping times for the 1.1 eV trap in these two detectors (given in Tables I and II), indicates that 1.1 eV trap is probably a hole trap and hence has negligible contribution to electron trapping, and hence $\mu\tau_e$. This analysis strengthens our suggestion of hole-type nature of 1.1 eV trap, which is originated from small Te precipitates. Further evidence will be acquired to investigate the nature of the 1.1 eV trap.

Fig. 5 shows that point defects exhibit the reverse behavior for de-trapping time, as shown for the trapping-time; there is an exponential increase for the de-trapping times with the traps' energy. The deep trap with 1.1 eV energy has the longest de-trapping time of about ~12 h.

Our quantitative analysis and statistics led us to conclude that, compared to shallow traps, deep traps take much shorter time to capture charge carriers and a longer time to release them, which suggests that deep traps play the dominant role in charge carriers' lifetimes. In addition, the nature of the trap (e or h), its concentrations, and capture cross-section must be taken into account in analyzing their effects on the lifetime for electrons and holes and the performance of the detector.

IV. CONCLUSIONS

We characterized the point defects in two different types of CTS detectors fabricated from high-quality crystals grown by the travelling heater method. The i-DLTS results revealed six different energy traps, including one shallow (metallic impurities), two A-centers with different origins (In- and Al-impurities), V_{Cd}^{--}, and two above-room-temperature deep traps. One of the deep traps is close to the mid-band gap, and the second being a Te-precipitates-related trap at 1.1 eV. We compared, for two detectors, the traps' capture cross sections, concentrations, times for trapping and de-trapping of the charge carriers, and related bulk resistivity and $\mu\tau_e$ product. From this data, we concluded that high densities of A-centers, V_{Cd}^{--}, and deep traps with binding energies of 0.87 eV play a dominant role in lowering the lifetime. The data analysis for the 1.1 eV trap makes one point clear, viz., that this trap may be the reason for high resistivity by pinning down the Fermi level, but, at the same time, it contributes towards the generation of space charge, and hence, the degradation of the detectors' performance. In addition, the capture cross-sections and densities of the 0.87 and 1.1 eV deep traps, mainly affect the trapping and de-trapping times of the charge carriers. However, we can assure the high values of $\mu\tau_e$ product and resistivity by controlling the energy traps and their concentrations, which makes CTS a potential candidate as alternative material for radiation-detector applications.

ACKNOWLEDGMENTS

This work was supported by the U.S. Department of Energy, Office of Defense Nuclear Nonproliferation Research and Development, DNN R&D. The manuscript was authored by Brookhaven Science Associates, with the U.S. Department of Energy. This work was partly supported by the U.S. Department of Homeland Security, Domestic Nuclear Detection Office, under competitively awarded contract/IAA Award No. 2012-DN-077-ARI065-03.

[1]"Cadmium zinc telluride spectrometers for gamma and X-Ray applications," in *Semiconductors for Room Temperature Nuclear Detector Applications*, edited by R. B. James, T. E. Schlesinger, J. C. Lund *et al.* (Academic, New York, 1995), Vol. 43, p. 334.
[2]T. E. Schlesinger, J. E. Toney, H. Yoon *et al.*, Mater. Sci. Eng. R **32**, 103 (2001).
[3]C. Szeles, IEEE Trans. Nucl. Sci. **51**(3), 1242 (2004).
[4]U. N. Roy, A. E. Bolotnikov, G. S. Camarda *et al.*, APL Mater. **3**, 026102 (2015).
[5]R. Gul, R. B. James, K. H. Kim *et al.*, J. Electron. Mater. **40**(3), 274 (2011).
[6]A. E. Bolotnikov, S. Babalola, G. S. Camarda *et al.*, IEEE Trans. Nucl. Sci. **58**(4), 1972 (2011).
[7]U. N. Roy, A. E. Bolotnikov, G. S. Camarda *et al.*, J. Cryst. Growth **43**, 386 (2014).
[8]R. Gul, U. N. Roy, A. E. Bolotnikov *et al.*, APL Mater. **3**, 040702 (2015).
[9]R. Gul, A. E. Bolotnikov, G. S. Camarda *et al.*, J. Appl. Phys. (submitted).
[10]H. Elhadidy, J. Franc, P. Moravec *et al.*, Semicond. Sci. Technol. **22**, 537 (2007).
[11]M. Fiederle, V. Babentsov, J. Franc *et al.*, J. Cryst. Growth **243**, 77 (2002).

[12]M. Fiederle, A. Fauler, V. Babentsov *et al.*, Nucl. Instrum. Methods Phys. Res., Sect. A **509**, 70 (2003).
[13]J. Z′azvorka, J. Franc, V. Dědič *et al.*, 15th International Workshop on Radiation Imaging Detectors, Paris, France, 2013.
[14]G. S. Camarda, A. E. Bolotnikov, Y. Cui *et al.*, IEEE Trans. Nucl. Sci. **55**(6), 3725 (2008).
[15]R. Gul, S. Egarievwe, G. Prekas *et al.*, "Study of point defects in As-grown and annealed Bridgman grown CZT crystals and their effects on $\mu\tau_e$-product and resistivity," Presentation in Hard X-ray and gamma-ray Detectors Physics, SPIE, San Diego, USA, 2014.
[16]A. Castaldini, A. Cavallini, B. Fraboni *et al.*, J. Appl. Phys. **83**(4), 2121 (1998).
[17]G. Tepper, R. Kessick, and C. Szeles, Proc. SPIE **4507**, 79 (2001).